Digital Twin Modeling Method of Three-Phase Inverter-Driven PMSM Systems for Parameter Estimation

Wensheng Song, *Senior Member, IEEE*, Yuchao Zou, Chenwei Ma, *Member, IEEE*, and Sihui Zhang, *Student Member, IEEE*

***Abstract*—This article proposes a digital twin modeling method of a three-phase inverter-driven permanent magnet synchronous motor (PMSM) for system parameter estimation offline, which does not require any signal injection or additional sensor and measuring equipment, resulting in a noninvasive approach for the digital modeling and parameter estimation of three-phase PMSM. In the proposed method, a digital twin model that includes the inverter-driven PMSM power stage and the close-loop controller is established in a first step. The key parameters of the PMSM (e.g., stator resistance, stator inductance, and flux linkage) are then obtained with a chaotic particle swarm optimization algorithm by comparing the output data of the digital twin model and the actual physical circuit. To verify the correctness of the proposed digital twin model, a series of experimental studies at different operating conditions are performed. In addition, the effectiveness of the parameter estimation based on the digital twin model has been confirmed, and the accuracy of the estimated parameters is acceptable.**

***Index Terms*—Chaos particle swarm optimization (PSO), digital twin, parameter estimation, permanent magnet synchronous motor (PMSM), three-phase inverter.**

I. Introduction

THE permanent magnet synchronous motor (PMSM) has found broad application in numerous fields owing to its high power density, exceptional efficiency, and excellent controllability, such as rail traction transportation [1] and electric vehicles [2]. The parameters of PMSMs are highly significant in motor control and condition monitoring [3], [4]. However, motor manufacturers usually do not disclose critical motor parameters such as stator resistance, inductance, and flux linkage. Additionally, the motor parameters vary depending on the operating conditions [5], [6]. Therefore, it is necessary to adopt appropriate parameter estimation methods to obtain the parameters of PMSMs.

Several parameter estimation methods have already been proposed. In the past, machine parameters were typically obtained using measurement instruments. Da et al. [7] proposed an approach to health monitoring and multifault detection in permanent magnet synchronous machines using direct flux measurement with search coils. Wang et al. [8] utilized a frequency analyzer to analyze the standstill frequency response of the PMSM and obtain the parameters. The main parameters of a permanent magnet motor, such as torque constant and d-axis and q-axis inductance L_d and L_q, can be obtained by measuring the machine torque during testing [9]. However, these methods relying on measurement tools are subject to the precision of the equipment and can significantly increase costs.

Therefore, it is necessary to use methods that can estimate the required parameters using signals that can be measured by existing sensors. Algorithms such as recursive least-squares (RLS) [10], [11], extended Kalman filter (EKF) [12], [13], and model reference adaptive system [14], [15] are applied to parameter estimation. Liu et al. [10] employ the RLS method to estimate stator resistance and d-q axis inductances, but the flux linkage is assumed constant. In [12], the EKF was used to estimate the stator resistance and flux linkage. The MARS method proposed in [14] and [15] cannot estimate multiparameters simultaneously. The MARS method requires nominal values of the parameters to estimate their actual values, but these nominal values are usually unknown and vary with operating conditions. It can be seen that the methods mentioned above are only able to obtain part of the parameters. Therefore, in [16], high-frequency voltage injection was used to obtain the high-frequency characteristics and increase the state equation, enabling multiparameter estimation. In [17], the parameters of the PMSM are identified by injecting a square wave current on the d-axis. First, the resistance and flux linkage are identified, followed by the estimation of the d,q-axis inductances. It can be seen that using signal injection is an effective method to achieve parameter estimation. However, additional injected signals may not only cause fluctuations in current and speed, affecting

Manuscript received 28 April 2023; revised 12 August 2023 and 11 October 2023; accepted 20 October 2023. Date of publication 6 November 2023; date of current version 22 December 2023. This work was supported in part by National Natural Science Foundation of China under Grant 52022084, in part by Sichuan Youth Science and Technology Innovation Research Team Project under Grant 22CXTD0055, and in part by the Scientific and Technological R&D Plan from China National Railway Group Limited under Grant K2023J008. Recommended for publication by Associate Editor F. Luo. *(Corresponding author: Wensheng Song.)*

The authors are with the School of Electrical Engineering, Southwest Jiaotong University, Chengdu 611756, China (e-mail: songwsh@swjtu.edu.cn; zouyuchao@my.swjtu.edu.cn; chenwei.ma@swjtu.edu.cn; zhangsh@my.swjtu.edu.cn).

Color versions of one or more figures in this article are available at https://doi.org/10.1109/TPEL.2023.3330240.

Digital Object Identifier 10.1109/TPEL.2023.3330240

control performance [18], but also cause parameter variations [19]. Moreover, researchers are interested in observer-based methods due to their simplicity to implement, such as adaptive observers (AOs), sliding-mode observers (SMOs), and disturbance observers [20], [21], [22], [23], [24]. In [20], an AO was designed for estimating the stator resistance and stator inductance of PMSMs. And the mechanical parameters are estimated by the SMO [22]. However, observer-based methods are not stable enough and are easily influenced by operating conditions.

Additionally, artificial intelligence is a solution for parameter estimation [25], [26], [27]. In [25], artificial neural networks (ANNs) such as feedforward and recurrent networks are used to estimate the parameters of induction motor. And a method combining Elman neural network and modified EKF was used to identify the stator resistance and stator flux of PMSMs [26]. Moreover, a physics-informed neural network that integrates physical models into data-driven pipelines is used for parameter estimation in dc–dc Buck converters [27]. The physical knowledge of the Buck converter is seamlessly integrated into the training of a deep neural network. However, ANNs require a large amount of offline training data, which is difficult to obtain in practice [28].

Digital twin is a virtual replica that corresponds to a real-world system and can simulate system behavior for monitoring, prediction, and optimization of system operation status, performance, and health [29]. Recently, digital twin has been applied to various fields, but there are few literatures in the field of power electronics. In [30] and [31], fault diagnosis of the power converters method is proposed, which is achieved by comparing the outputs of the digital twin with those of the physical twin. And in [32] and [33], a digital twin-based parameter estimation method is applied in Buck converters. Wu et al. [34] and Shi et al. [35] show digital twin models of single-phase and three-phase inverters, respectively, but they are used for resistive and inductive loads without motors. [36], [37], and [38] show the digital twin model of PMSMs, however the entire closed-loop system, such as the control system and the inverter, is not involved.

In this article, a digital twin model of a three-phase inverter-driven PMSM is established. Based on this digital twin model, a parameter estimation method for PMSM is proposed. The rest of this article is organized as follows. Section II primarily describes the composition and operation of the closed-loop system and models the three-phase inverter and PMSM. Section III introduces intelligent optimization algorithms to optimize the model and obtain the parameters of PMSM. In Section IV, an experimental prototype of a three-phase inverter-driven PMSM is developed to verify the correctness of the proposed digital twin model and the parameter estimation method. Finally, Section V concludes the article.

The main contributions of this article are summarized as follows.

1) By utilizing existing control signal data, a digital twin model of the three-phase PMSM by a three-phase two-level inverter is established, which can be used to obtain the operating state of the actual physical system.
2) The key parameters of PMSM are obtained under different operating conditions, which provide possibilities for achieving high-performance control and condition monitoring of PMSM.
3) The proposed method is nonintrusive without injecting additional signals or extra sensors and equipment.

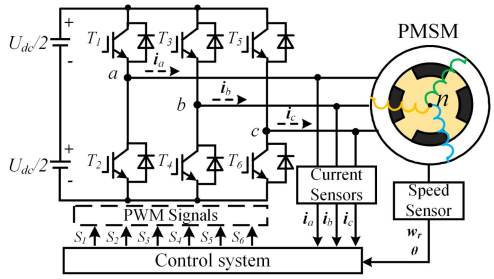

Fig. 1. Topology of three-phase two-level inverter-driven PMSM systems.

II. Digital Model of Three-Phase Inverter and PMSM

A. Modeling of Three-Phase Inverter-Driven PMSM System

The topology of a three-phase two-level inverter drive PMSM is shown in Fig. 1, where T_1–T_6 are power switches; U_{dc} is the dc-link voltage.

Therefore, the three-phase inverter output phase voltage is represented by

$$\begin{cases} U_{an} = \frac{2}{3}(S_1A_1 + S_2\mathrm{A}_2) - \frac{1}{3}(S_3B_1 + S_4B_2) \\ \qquad -\frac{1}{3}(S_5C_1 + S_6C_2) \\ U_{bn} = -\frac{1}{3}(S_1A_1 + S_2\mathrm{A}_2) + \frac{2}{3}(S_3B_1 + S_4B_2) \\ \qquad -\frac{1}{3}(S_5C_1 + S_6C_2) \\ U_{cn} = -\frac{1}{3}(S_1A_1 + S_2\mathrm{A}_2) - \frac{1}{3}(S_3B_1 + S_4B_2) \\ \qquad +\frac{2}{3}(S_5C_1 + S_6C_2) \end{cases} \tag{1}$$

where U_{an}, U_{bn}, and U_{cn} are phase voltages; S_i are signals of switches (1 represents on-state, 0 represents off-state, where $i = 1, 2, 3, 4, 5, 6$), and two switches on the same bridge arm cannot be on at the same time ($S_1+S_2=0$, $S_3+S_4=0$, $S_5+S_6=0$); A_1, A_2, B_1, B_2, C_1, C_2 are represented by

$$\begin{cases} A_1 = \frac{U_{dc}}{2} i_{a,\mathrm{sign}} + \frac{U_{dc}}{2} \hat{i}_{a,\mathrm{sign}} \\ A_2 = -\frac{U_{dc}}{2} i_{a,\mathrm{sign}} - \frac{U_{dc}}{2} \hat{i}_{a,\mathrm{sign}} \\ B_1 = \frac{U_{dc}}{2} i_{b,\mathrm{sign}} + \frac{U_{dc}}{2} \hat{i}_{b,\mathrm{sign}} \\ B_2 = -\frac{U_{dc}}{2} i_{b,\mathrm{sign}} - \frac{U_{dc}}{2} \hat{i}_{b,\mathrm{sign}} \\ C_1 = \frac{U_{dc}}{2} i_{c,\mathrm{sign}} + \frac{U_{dc}}{2} \hat{i}_{c,\mathrm{sign}} \\ C_2 = -\frac{U_{dc}}{2} i_{c,\mathrm{sign}} - \frac{U_{dc}}{2} \hat{i}_{c,\mathrm{sign}} \end{cases} \tag{2}$$

where $i_{k,\mathrm{sign}}$ are the direction of phase currents (1 represents the phase current direction shown in Fig. 1, and 0 is the opposite, where $k = a, b, c$), and $i_{k,\mathrm{sign}} + \hat{i}_{k,\mathrm{sign}} = 0$.

In addition, the model of PMSM under the dq-axis is

$$\begin{cases} \frac{di_d}{dt} = \frac{1}{L_d} U_d - \frac{R}{L_d} i_d + \omega_e \frac{L_q}{L_d} i_q \\ \frac{di_q}{dt} = \frac{1}{L_q} U_q - \frac{R}{L_q} i_q - \omega_e \frac{L_d}{L_q} i_d - \omega_e \frac{1}{L_q} \psi_f \end{cases} \tag{3}$$

where $U_{d,q}$ are dq-axis voltages; $i_{d,q}$ are dq-axis currents; ω_e is electrical angular speed; $L_{d,q}$ are stator inductances ($L_d = L_q$); R is stator resistance; ψ_f refers to the flux linkage. The quantities in the d-q coordinate can be obtained by the a-b-c coordinate with the rotor position angle, which can be described as

$$\begin{bmatrix} d \\ q \end{bmatrix} = \begin{bmatrix} \cos\theta_e & \sin\theta_e \\ -\sin\theta_e & \cos\theta_e \end{bmatrix} \begin{bmatrix} \frac{2}{3}\left(a - \frac{1}{2}b - \frac{1}{2}c\right) \\ \frac{2}{3}\left(\frac{\sqrt{3}}{2}b - \frac{\sqrt{3}}{2}c\right) \end{bmatrix} \tag{4}$$

where θ_e is the rotor position angle.

In this article, the linearization of differential equations using the fourth-order Runge-Kutta method, (3) is rewritten as follows:

$$\begin{cases} i_{d,n+1} = i_{d,n} + \frac{h}{6}\left(K_{a1} + 2K_{a2} + 2K_{a3} + K_{a4}\right) \\ i_{q,n+1} = i_{q,n} + \frac{h}{6}\left(K_{b1} + 2K_{b2} + 2K_{b3} + K_{b4}\right) \end{cases} \tag{5}$$

where $i_{d,n+1}$, $i_{q,n+1}$, and $i_{d,n}$, $i_{q,n}$ are the currents at (n+1)th step and (n)th step respectively; h is the calculation step from (n)th step to (n + 1)th step, which is set to 1e-7s in this article; K_{a1}-K_{a4} and K_{b1}-K_{b4} are the coefficients, which are shown as follows:

$$\begin{cases} K_{a1} = f_1\left(i_{d,n}, i_{q,n}\right) \\ K_{b1} = f_2\left(i_{d,n}, i_{q,n}\right) \\ K_{a2} = f_1\left(i_{d,n} + \frac{h}{2}K_{a1}, i_{q,n} + \frac{h}{2}K_{b1}\right) \\ K_{b2} = f_2\left(i_{d,n} + \frac{h}{2}K_{a1}, i_{q,n} + \frac{h}{2}K_{b1}\right) \\ K_{a3} = f_1\left(i_{d,n} + \frac{h}{2}K_{a2}, i_{q,n} + \frac{h}{2}K_{b2}\right) \\ K_{b3} = f_2\left(i_{d,n} + \frac{h}{2}K_{a2}, i_{q,n} + \frac{h}{2}K_{b2}\right) \\ K_{a4} = f_1\left(i_{d,n} + hK_{a3}, i_{q,n} + hK_{b3}\right) \\ K_{b4} = f_2\left(i_{d,n} + hK_{a3}, i_{q,n} + hK_{b3}\right) \end{cases}. \tag{6}$$

Substitute (3) into (6), and (6) into (5), then the model can be described as

$$\begin{bmatrix} i_{d,n+1} \\ i_{q,n+1} \end{bmatrix} = \begin{bmatrix} f_1\left(L_d, L_q, R, S_{1\sim6}\right) \\ f_2\left(L_d, L_q, R, \psi_f, S_{1\sim6}\right) \end{bmatrix} \begin{bmatrix} i_{d,n} \\ i_{q,n} \\ \omega_{e,n} \end{bmatrix} \tag{7}$$

where L_d, L_q, R, and ψ_f are unknown parameters; S_{1-6} are the signals of switches. Therefore, the dq-axis currents at the (n + 1)th step can be obtained by dq-axis currents and electrical angular speed at the (n)th step. Then, the currents in the a-b-c coordinate can be calculated by the inverse transformation of (4) and shown as

$$\begin{bmatrix} a \\ b \\ c \end{bmatrix} = \begin{bmatrix} d \\ q \end{bmatrix} \begin{bmatrix} \cos\theta_e & -\sin\theta_e \\ \sin\theta_e & \cos\theta_e \end{bmatrix} \begin{bmatrix} 1 & 0 \\ -1/2 & \sqrt{3}/2 \\ -1/2 & \sqrt{3}/2 \end{bmatrix}. \tag{8}$$

B. Close-Loop Controller

The three-phase two-level inverter has eight switching states, which correspond to eight voltage vectors. Six of them are effective voltage vectors (u_1-u_6) and two are zero vectors (u_0,u_7), as shown in Fig. 2.

In this article, the model predictive current control (MPCC) strategy is used to control the motor due to its simple implementation and good dynamic performance. The control block diagram is shown in Fig. 3.

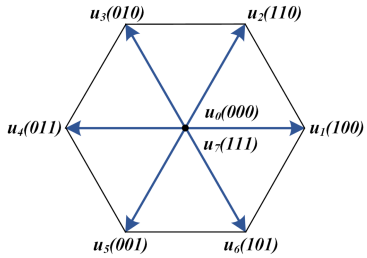

Fig. 2. Space voltage vectors of a three-phase two-level inverter.

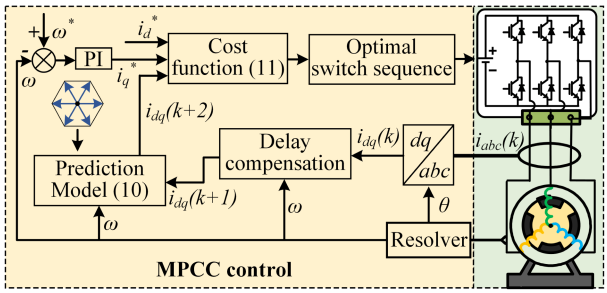

Fig. 3. Block diagram of the MPCC scheme.

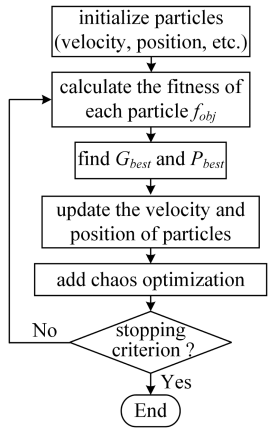

Fig. 4. Executing procedure of the adopted CPSO algorithm.

PI controller is adopted for the outer loop of rotational speed and MPCC method is adopted for the inner loop of current. The q-axis current command value is obtained from the difference between the actual speed and the given speed by the output of the PI controller and the d-axis current command value is generally set to zero, which is shown as

$$\begin{cases} \omega_{\mathrm{err},k+1} = \omega_{\mathrm{ref}} - \omega_{e,k+1} \\ i^*_{q,k+1} = i^*_{q,k} + K_p\left(\omega_{\mathrm{err},k+1} - \omega_{\mathrm{err},k}\right) + K_I T\omega_{\mathrm{err},k+1} \\ i^*_{d,k+1} = 0 \end{cases} \tag{9}$$

where k + 1 and k represent the next moment and the current moment, respectively; T is the control period; ω_{ref} is the reference of the rotor speed; ω_{err} is the error between the rotor speed

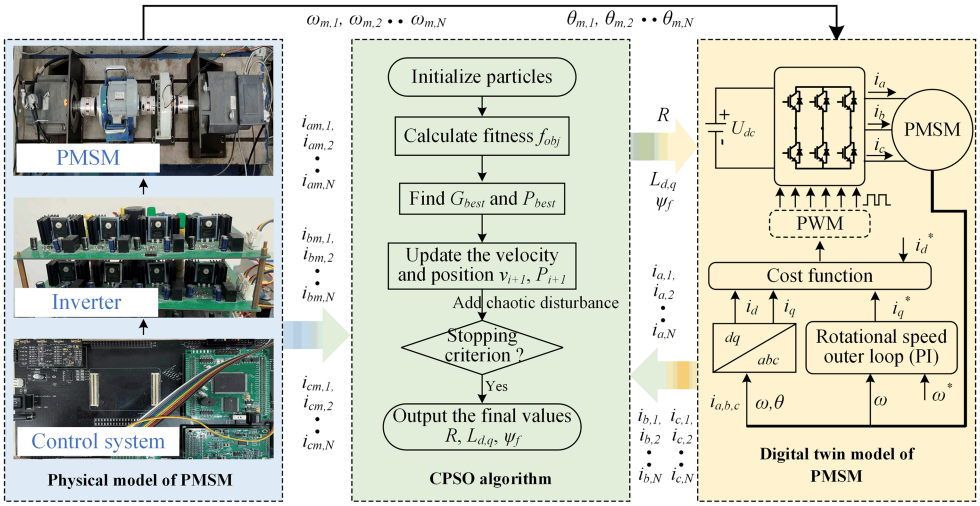

Fig. 5. Process of the digital twin-based parameter estimation of PMSM.

and its reference; K_p and K_I are the parameters of PI; $i_{d,q}^*$ are the dq-axis command currents.

According to (3), the predictive currents at the next step are obtained by using the forward Euler discretization equation as

$$\begin{bmatrix} i_d(k+1) \\ i_q(k+1) \end{bmatrix} = \begin{bmatrix} \left(1-\frac{TR}{L_d}\right) & T\omega_e \\ -T\omega_e & \left(1-\frac{TR}{L_q}\right) \end{bmatrix} \begin{bmatrix} i_d(k) \\ i_q(k) \end{bmatrix} + \begin{bmatrix} \frac{T}{L_d} & 0 \\ 0 & \frac{T}{L_q} \end{bmatrix} \begin{bmatrix} V_d(k) \\ V_q(k) \end{bmatrix} + \begin{bmatrix} 0 \\ -\frac{T}{L_q}\omega_e(k)\psi_f \end{bmatrix}. \tag{10}$$

And then, the corresponding predicted current values of different voltage vectors are obtained by (10) and substituting them into the cost function (11) to find the optimal voltage vector corresponding to the switching sequence acting on the inverter

$$g = \left(i_d^* - i_d\right)^2 + \left(i_q^* - i_q\right)^2. \tag{11}$$

In addition, the calculation delay needs to be compensated because the process of sampling, processing and execution of the signal in the actual system will consume a certain amount of time. However, it is not the focus of this article.

III. Application of Digital Twin in Parameter Estimation

The accuracy of the digital twin model depends on the model parameters. The intelligent algorithm continuously iterates on the parameters to correct them so that the digital twin gets closer and closer to the physical circuit and finally finds the internal model parameters of the circuit.

Particle swarm optimization (PSO) is a heuristic optimization algorithm with simple implementation and good generality, which is suitable for searching for the optimal parameters of digital twin PMSM. But PSO is prone to fall into local optimum.

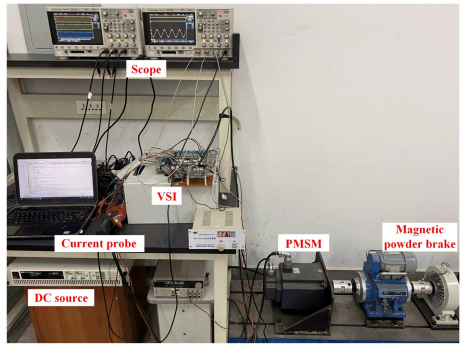

Fig. 6. Photograph of an experimental prototype.

TABLE I
Parameters of PMSM

Parameter	Symbol	Value
dc-link voltage	U_{dc}	250 V
Stator resistance	R	0.71 Ω
d-axis inductance	L_d	6.24 mH
q-axis inductance	L_q	6.24 mH
Flux linkage	ψ_f	0.420 Wb
Pole pairs	n_p	4
Switching frequency	f_s	10 kHz
Sampling frequency	f_{sr}	50 kHz

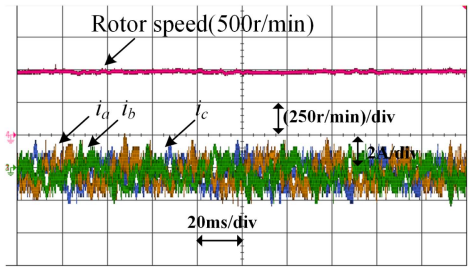

Fig. 7. Waveforms of three-phase currents and rotor speed under 1 N·m load torque at 500 r/min.

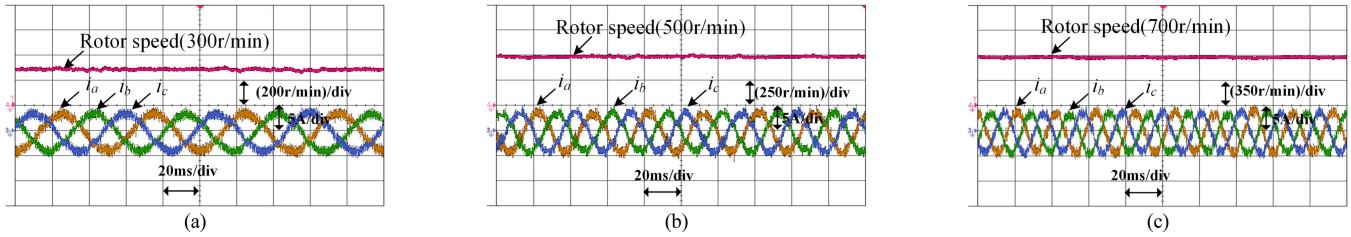

Fig. 8. Waveforms of three-phase currents and rotor speed under 9 N·m load torque. (a) 300 r/min. (b) 500 r/min. (c) 700 r/min.

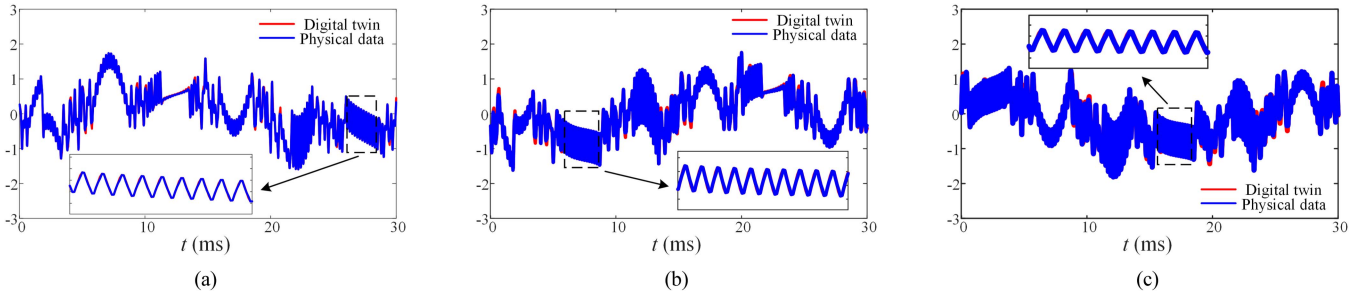

Fig. 9. Waveforms comparison of three-phase currents at 500 r/min under 1 N·m load torque. (a) A phase current. (b) B phase current. (c) C phase current.

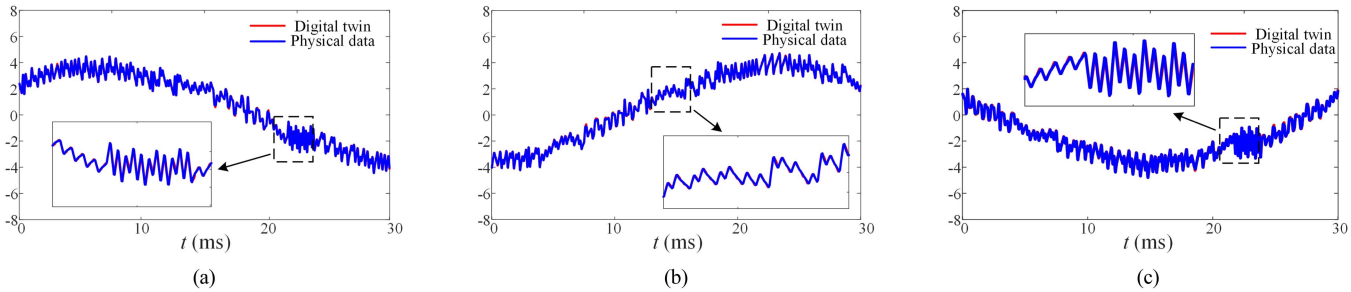

Fig. 10. Waveforms comparison of three-phase currents at 300 r/min under 9 N·m load torque. (a) A phase current. (b) B phase current. (c) C phase current.

To reduce the probability of falling into a local optimum, a CPSO algorithm based on the LOGISTIC equation is proposed.

To implement CPSO, the first step is to construct the objective function, the objective function is as follows:

$$f_{\text{obj}} = \frac{\sum_{j=1}^{N}\left[(i_{am,j}-i_{a,j})^2+(i_{bm,j}-i_{b,j})^2+(i_{cm,j}-i_{c,j})^2\right]}{N} \tag{12}$$

where i_a, i_b, i_c are the calculated phase currents from the digital twin PMSM; i_{am}, i_{bm}, i_{cm} are the measured data from the physical PMSM; N is the sample size of the measured data. The PMSM parameters are obtained by minimizing f_{obj} with CPSO [39].

Fig. 4 shows the executing procedure of the adopted CPSO algorithm. The basic characteristics of a particle are its position and velocity, which can be updated by the following equations:

$$\begin{cases} v_{i,j} = \omega_{i-1}v_{i-1,j} + c_1 r_{1,i-1,j}\left(P_{best} - P_{i-1,j}\right) \\ \qquad + c_2 r_{2,i-1,j}\left(G_{best} - P_{i-1,j}\right) \\ P_{i,j} = P_{i-1,j} + v_{i,j} \end{cases} \tag{13}$$

where i is the number of iterations, j is the number of particles, $v_{i,j}$ is the moving velocity of the (j)th particle in (i)th iteration; $P_{i,j}$ is the position of the (j)th particle in (i)th iteration; G_{best} and P_{best} represent the global best particle and the personal best particle respectively; ω, r_1, r_2, c_1, and c_2 are the parameters.

At first, initialization of all particles, including velocity and position, etc. The fitness of each particle is calculated by (12) and the G_{best} and P_{best} are found. Then, the velocity and position of the particles are updated in (13), and the fitness of the updated particles is calculated and the newest G_{best} and P_{best} are found. And performing chaos optimization when a certain iteration is satisfied. The basic idea is: using the randomness, regularity, and ergodicity characteristics of chaos theory, the optimal solution found in the whole swarm is used as the initial value to generate

TABLE II
PARAMETERS ESTIMATION RESULTS

Number	$R(\Omega)$	$L_{d,q}$(mH)	ψ_f(Wb)
1	0.7572	6.451	0.4095
2	0.7801	6.365	0.4082
3	0.787	6.531	0.4091
4	0.7643	6.644	0.4098
5	0.7711	6.326	0.4088
Average	0.7719	6.463	0.40908
Nominal	0.71	6.24	0.421
error	8.72%	3.57%	2.8%

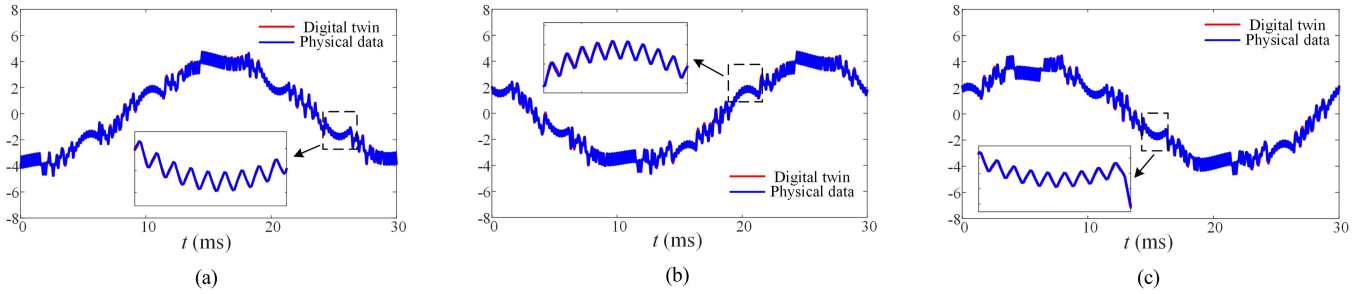

Fig. 11. Waveforms comparison of three-phase currents at 500 r/min under 9 N·m load torque. (a) A phase current. (b) B phase current. (c) C phase current.

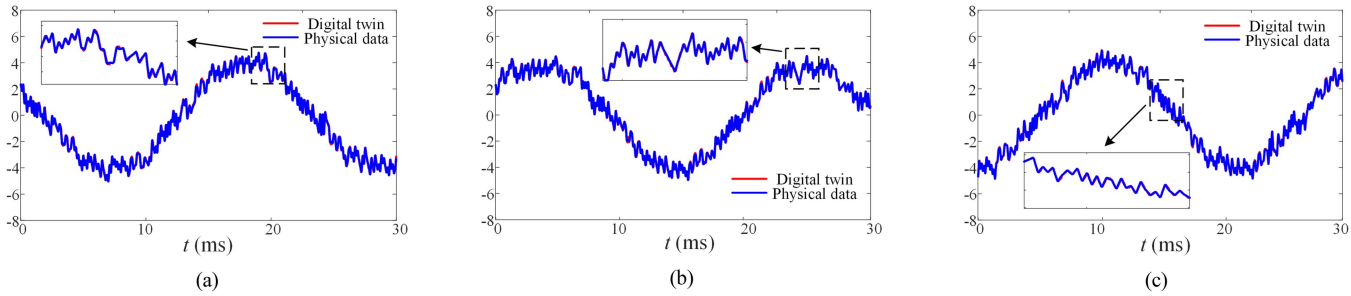

Fig. 12. Waveforms comparison of three-phase currents at 700 r/min under 9 N·m load torque. (a) A phase current. (b) B phase current. (c) C phase current.

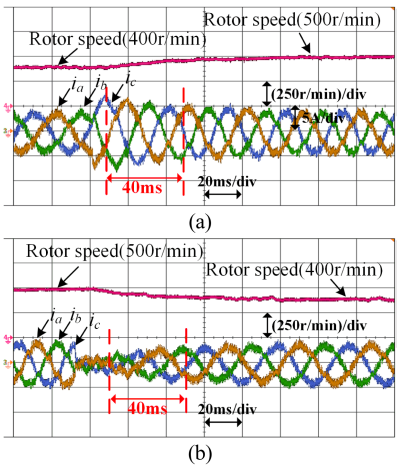

Fig. 13. Waveforms of three-phase currents and rotor speed when the rotor speed varies under 9 N·m load torque. (a) 400–500 r/min. (b) 500–400 r/min.

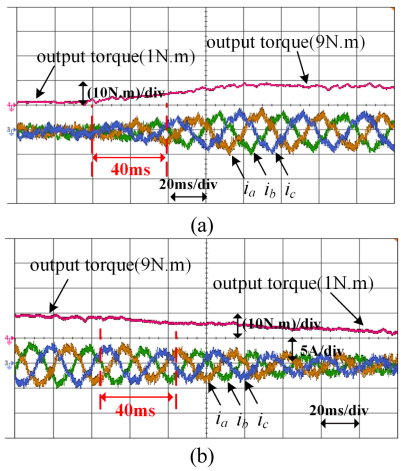

Fig. 14. Waveforms of three-phase currents and output torque when the load torque varies at 500 r/min rotor speed. (a) 1–9 N·m. (b) 9–1 N·m.

TABLE III
DIFFERENT OPERATING CONDITIONS

Number of case	Rotor speed (r/min)	Load torque (N.m)
1	300	9
2	500	9
3	700	9
4	500	1
5	400→500	9
6	500→400	9
7	500	1→9
8	500	9→1

TABLE IV
PARAMETERS ESTIMATION RESULTS

case	$R(\Omega)$	$L_{d,q}$(mH)	ψ_f(Wb)
1	0.7548	6.582	0.411
2	0.7719	6.4634	0.4091
3	0.7781	6.602	0.4083

a chaotic sequence, while the particle with the optimal value in the chaotic sequence is interchanged with the particle in the current particle swarm.

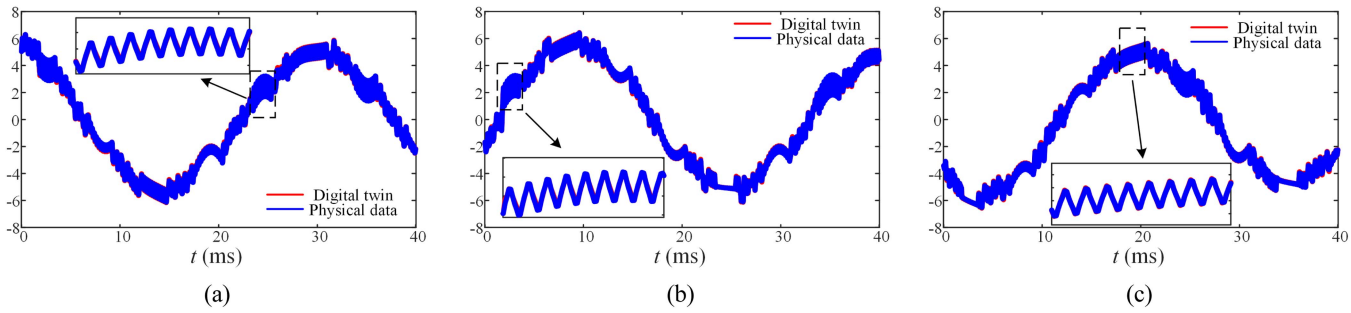

Fig. 15. Waveforms comparison of three-phase currents when the rotor speed varies from 400 to 500 r/min under 9 N·m load torque. (a) A phase current. (b) B phase current. (c) C phase current.

First, the position of the G_{best} particle is converted to the (0,1) interval by the following formula:

$$z_x = \frac{G_{\text{best},x} - a_x}{b_x - a_x}, x = 1, 2 \ldots \tag{14}$$

where x is the dimension of particles (number of parameters). b_x and a_x are the upper and lower bounds of particles, respectively.

Then, the chaotic sequence is obtained by LOGISTIC equation, which is shown as

$$z_{x,y+1} = \mu(1 - z_{x,y})z_{x,y}, y = 1, 2 \ldots \tag{15}$$

where $z_{x,y}$ represents the (x)th chaotic variable of the (y)th iteration; n is the number of chaotic sequences; μ is the control parameter usually taken as 4, and the whole system is in a completely chaotic state.

The chaotic sequence is returned to the particles in the original solution space:

$$P_{i,y} = z_y(b - a) + a. \tag{16}$$

The fitness is calculated in (12) again, and repeating the above process until the stopping criterion is met.

The process of the digital twin-based parameter estimation is shown in Fig. 5, which is implemented offline. The calculation of digital twin model and the realization of CPSO algorithm are all carried out on MATLAB platform. First**,** collect short-term experimental data (i_{a}, i_{b}, i_{c}, ω_{e}, θ) of actual physical circuits and import them into MATLAB workspace. Second, input the sampling values of the actual physical circuit data and circuit parameters (unknown parameters: $R_{\text{s}}, L_{\text{d,q}}, \psi_{\text{f}}$) into the closed-loop system's digital twin model as the initial values, and the external characteristic data ($i_{\text{a}}, i_{\text{b}}, i_{\text{c}}$) can be obtained from the digital twin model. Finally**,** the circuit parameters are continuously iterated and optimized through using the CPSO algorithm. When the objective function is smaller than the predefined threshold, the final digital twin model and the actual circuit parameters can be obtained.

With the CPSO algorithm as a bridge, the physical counterpart and the digital twin are connected, and the internal parameters of the physical PMSM are obtained by iteratively modifying the digital twin.

IV. Experimental Verification

A. Experimental Platform

To verify the proposed digital twin method for parameter estimation, an experimental prototype of a three-phase two-level inverter-driven PMSM is built, as shown in Fig. 6. In this platform, the control methods are programmed and implemented in TI DSP TMS320F28335. The LA55-P current sensors produced by LEM company are used in the experimental platform. The RDC chip AD2S1200 produced by Analog Devices Inc. company is used to detect the rotor position and speed of the motor. The parameters of PMSM are listed in Table I.

B. Digital Twin Model Verification

1) Steady-State Performance: Fig. 7 shows the oscilloscope waveforms of three-phase currents and rotor speed in a steady state, where the load torque is 1 N·m. And Fig. 8 shows the oscilloscope waveforms of three-phase currents and rotor speed under 9 N·m load torque. The speed can meet the given speed and the three-phase currents are sinusoidal, which indicates that the motor is operating normally. Figs. 9–12 show the digital twin phase-current waveforms compared with the actual phase-current waveforms. It is worth noting that the actual three-phase current values are obtained by the controller sampling value, which does not require additional sensors. The time interval is the same under different operating conditions.

2) Dynamic Performance: The actual operating conditions are variable and the digital twin model must be the same as the actual circuit dynamics. Therefore, under the condition of 9 N·m load torque, varying the reference rotor speed from 400 to 500 r/min and varying the reference rotor speed from 500 to 400 r/min, the waveform is shown in Fig. 13. Then, when the rotor speed is 500 r/min, the load torque is changed from 1 to 9 N·m and from 9 to 1 N·m, as shown in Fig. 14.

Figs. 15–18 show the digital twin phase-current waveforms compared with the actual phase-current waveforms. It can be seen that the digital twin model has the same external characteristics as the physical prototype even during the dynamic process.

Therefore, the digital twin model of three-phase inverter-driven PMSM systems is accurate enough in external characteristics. It can be used for parameter estimation of PMSMs.

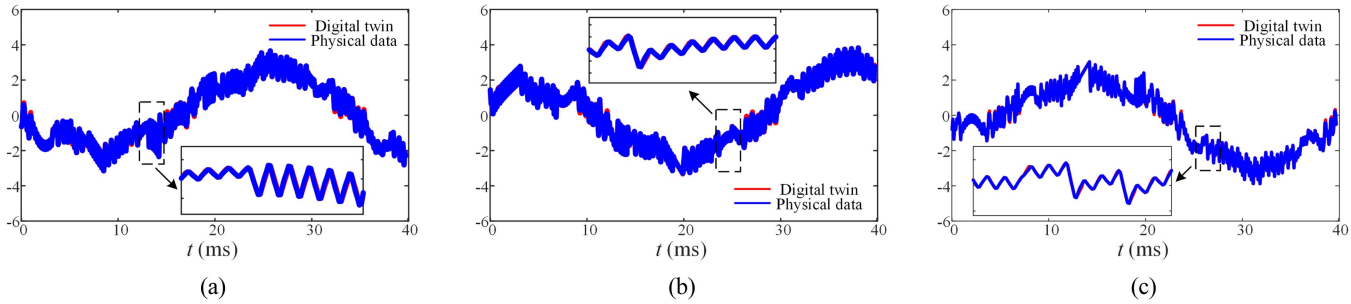

Fig. 16. Waveforms comparison of three-phase currents when the rotor speed varies from 500 to 400 r/min under 9 N·m load torque. (a) A phase current. (b) B phase current. (c) C phase current.

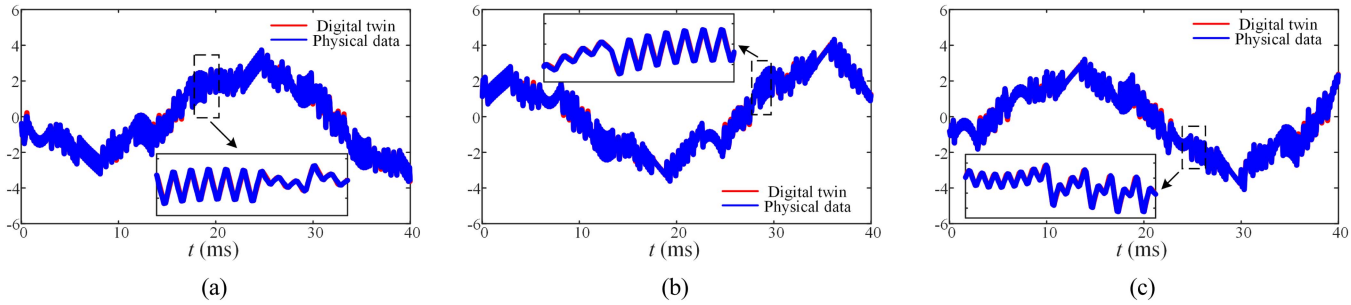

Fig. 17. Waveforms comparison of three-phase currents when the load torque varies from 1 to 9 N·m at rotor speed 500 r/min. (a) A phase current. (b) B phase current. (c) C phase current.

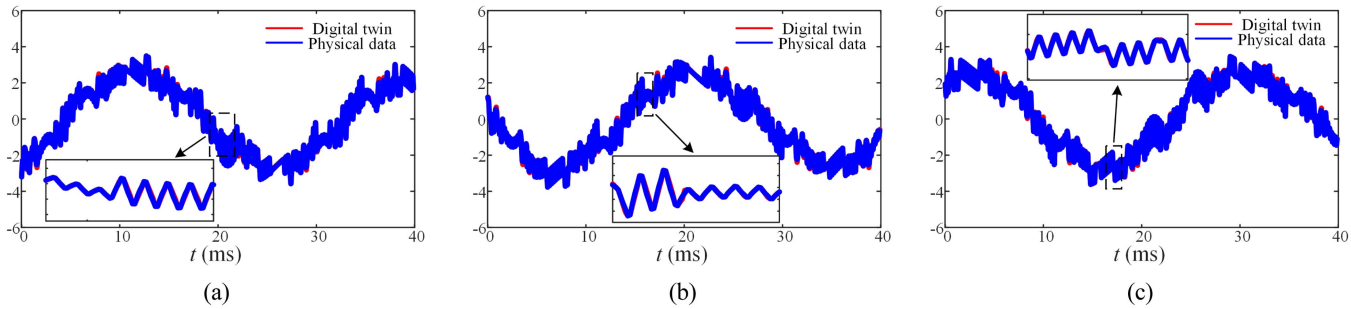

Fig. 18. Waveforms comparison of three-phase currents when the load torque varies from 9 to 1 N·m at rotor speed 500 r/min. (a) A phase current. (b) B phase current. (c) C phase current.

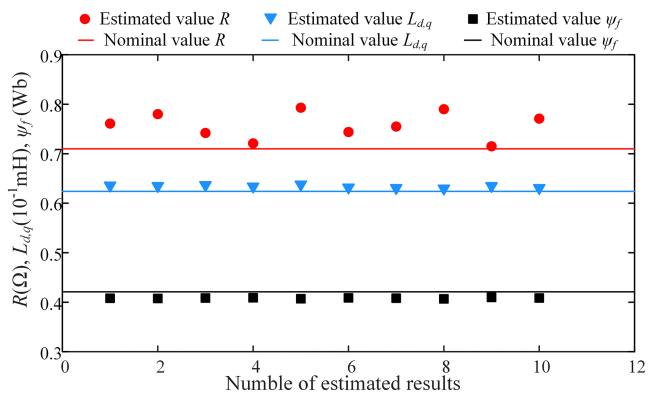

Fig. 19. Results of parameters estimation.

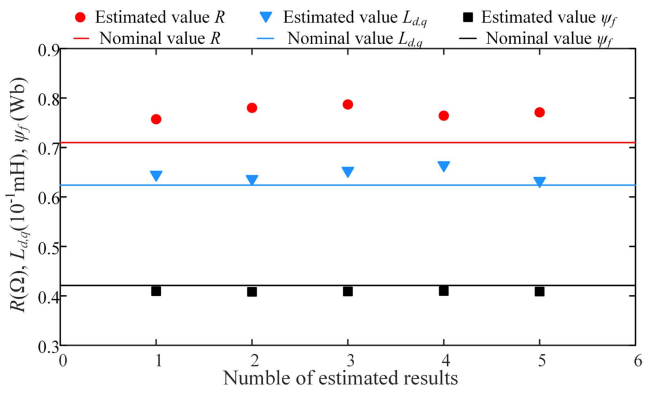

Fig. 20. Average value of parameters estimation.

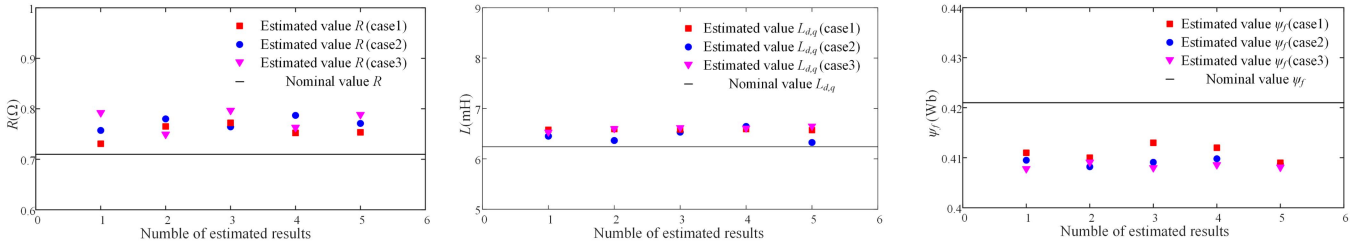

Fig. 21. Results of parameters estimation under different rotor speeds. (a) R. (b) $L_{d,q}$. (c) ψ_f.

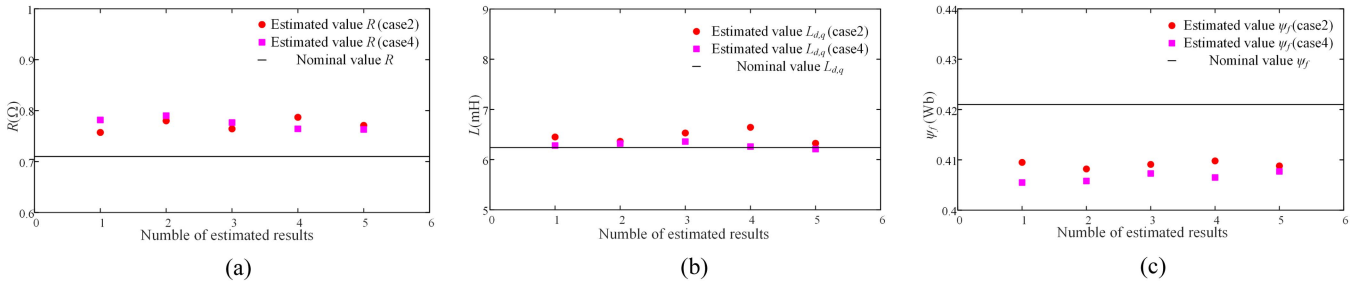

Fig. 22. Results of parameters estimation under different load torque. (a) R. (b) $L_{d,q}$. (c) ψ_f.

C. Parameter Estimation of PMSM

The accuracy of the model parameters is an important accuracy indicator of the established digital twin model. To further verify the accuracy of the digital twin model, the parameters of the PMSM are obtained according to the procedure shown in Fig. 5. To avoid the influence of temperature variation, the data are collected immediately after the motor starts. It is worth noting that before starting the motor next time, the motor and IGBT are dissipated to ensure that the experimental prototype runs at the same temperature as far as possible.

Fig. 19 shows the estimation results under steady-state conditions, where the rotor speed is 500 r/min and the load torque is 9 N·m. The procedure in Fig. 5 is performed 10 times.

To further verify the accuracy of the method, the motor prototype is run 5 times and the data are collected. Each set of data is used for parameter estimation 10 times, and the average value of parameters is obtained which is shown in Fig. 20 and Table II. The average error of resistance estimation is 7.8%. The estimation errors of inductance and flux linkage are 3.57% and 2.8% respectively. The estimation results are considered as the average value within 30 ms, and the errors are within the acceptable range.

D. Different Operating Conditions

In fact, the operating conditions of the motor are diverse, and its speed and load are different. To further verify the method, parameter estimation at different speeds and load torques is performed. And Table III shows the different operating conditions of the prototype.

1) Different Rotor Speeds: As with the steps in Section IV-C, the parameter estimation results of cases 1–3 are obtained, as shown in Fig. 21. The average values of all parameters are listed in Table IV.

2) Different Load Torques: The parameter estimation results of case 2 and case 4 are shown in Fig. 22. The average values of all parameters are listed in Table V.

For the transient process (case 5–8), 40 ms data in Figs. 13 and 14 are used, and the average values of all parameters are listed in Table VI.

TABLE V
PARAMETERS ESTIMATION RESULTS

Case	$R(\Omega)$	$L_{d,q}$(mH)	ψ_f(Wb)
2	0.7719	6.4634	0.4091
4	0.7752	6.2860	0.4066

TABLE VI
PARAMETERS ESTIMATION RESULTS

Case	$R(\Omega)$	$L_{d,q}$(mH)	ψ_f(Wb)
5	0.7788	6.351	0.409
6	0.7812	6.457	0.4121
7	0.7754	6.312	0.4089
8	0.7651	6.365	0.4095

E. Impact of Other Factors

1) DC-Link Voltage: Fig. 23 shows the results of parameter estimation under different dc-link voltages.

2) Parameter Mismatch: Motor parameters are needed in (10) in MPCC control. The control performance will deteriorate and the current will be worse when the motor parameters used in the control do not match the actual parameters. In this article, the inductance parameter of DSP controller is changed to 2.5 times the nominal value, and the inductance parameter of the

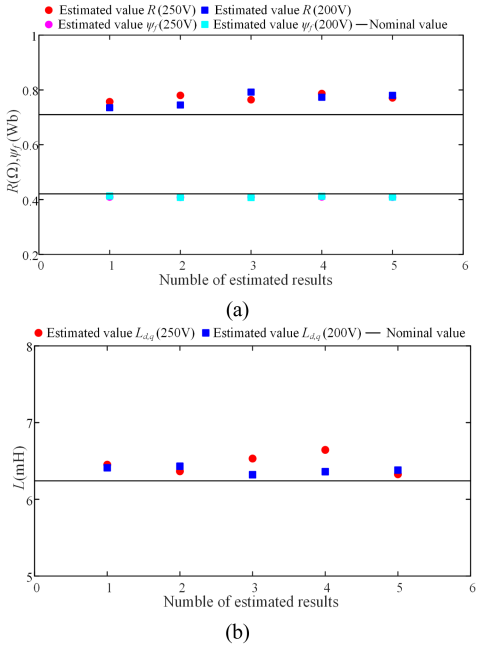

Fig. 23. Results of parameters estimation under different DC-link voltages. (a) R and ψ_f. (b) $L_{d,q}$.

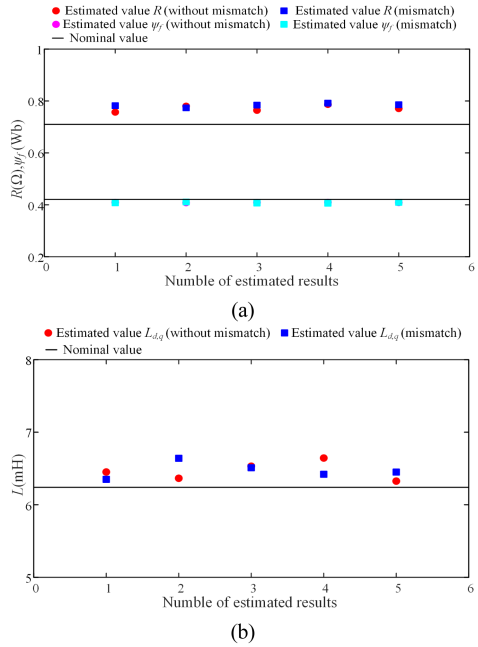

Fig. 24. Results of parameters estimation with the inductance parameter mismatch. (a) R and ψ_f. (b) $L_{d,q}$.

controller in the digital twin model is also changed to 2.5 times the nominal value. The parameter estimation results are shown in Fig. 24.

And the results of parameter estimation when different parameters mismatches are introduced are shown in Table VII. R_0, L_0, and ψ_{f0} are nominal parameters values, and R_c, L_c, and ψ_{fc} are control parameter values.

TABLE VII
PARAMETERS ESTIMATION RESULTS

Case	$R(\Omega)$	$L_{d,q}$(mH)	ψ_f(Wb)
R_c=2R_0, L_c=L_0, ψ_{fc}=ψ_{f0}	0.8223	6.652	0.4052
R_c=R_0, L_c=L_0, ψ_{fc}=1.6ψ_{f0}	0.7982	6.989	0.4018
R_c=R_0, L_c=2.5L_0, ψ_{fc}=1.6ψ_{f0}	0.8148	6.721	0.4064

V. CONCLUSION

In this article, a digital twin model of a three-phase PMSM driven by a three-phase two-level inverter is established, and the output characteristics of the proposed digital twin model are verified under steady state and dynamic conditions, which are similar to those of the actual physical prototype. Then, on the basis of the digital twin model, a parameter estimation approach of the key motor parameters including stator resistance, *dq*-axis inductance and flux linkage, is proposed. The feasibility of the parameter estimation method is verified by experimental tests under different operating conditions. The salient features of the proposed digital twin model and parameter estimation method are shown as follows.

1) A digital twin model of a three-phase two-level inverter-driven PMSM system is developed, including the motor model, the main inverter circuit, and the whole closed-loop control system with the DSP controller.
2) Parameter estimation results are counted and averaged to reduce the error of the estimation results, the stator resistance error between estimated value and nominal value is less than 10%, and the errors of *dq*-axis inductance and flux linkage are about 5%.
3) Under various operating conditions including different rotor speeds and load torques, the parameter estimation method remains effective, and the estimated parameters are acceptable. And it is not affected by the dc-link voltage or parameter mismatch.
4) The proposed method can be implemented only using the data from the existing sensors without signal injection or additional sensor.

Therefore, the proposed parameter estimation method of PMSM based on the digital twin model is effective under different operating conditions. It is a noninvasive approach for parameter estimation of PMSMs.

REFERENCES

[1] S. Lin, X. Fang, X. Wang, Z. Yang, and F. Lin, "Multi-objective model predictive current control method of permanent magnet synchronous traction motors with multiple current bounds in railway application," *IEEE Trans. Ind. Electron.*, vol. 69, no. 12, pp. 12348–12357, Dec. 2022.
[2] K.-M. Choo and C.-Y. Won, "Design and analysis of electrical braking torque limit trajectory for regenerative braking in electric vehicles with PMSM drive systems," *IEEE Trans. Power Electron.*, vol. 35, no. 12, pp. 13308–13321, Dec. 2020.
[3] I. Hammoud et al., "On continuous-set model predictive control of permanent magnet synchronous machines," *IEEE Trans. Power Electron.*, vol. 37, no. 9, pp. 10360–10371, Sep. 2022.
[4] J. Faiz and E. Mazaheri-Tehrani, "Demagnetization modeling and fault diagnosing techniques in permanent magnet machines under stationary and nonstationary conditions: An overview," *IEEE Trans. Ind. Appl.*, vol. 53, no. 3, pp. 2772–2785, May/Jun. 2017.

[5] K. Liu, Z. Q. Zhu, and D. A. Stone, "Parameter estimation for condition monitoring of PMSM stator winding and rotor permanent magnets," *IEEE Trans. Ind. Electron.*, vol. 60, no. 12, pp. 5902–5913, Dec. 2013.
[6] S. J. Underwood and I. Husain, "Online parameter estimation and adaptive control of permanent-magnet synchronous machines," *IEEE Trans. Ind. Electron.*, vol. 57, no. 7, pp. 2435–2443, Jul. 2010.
[7] Y. Da, X. Shi, and M. Krishnamurthy, "A new approach to fault diagnostics for permanent magnet synchronous machines using electromagnetic signature analysis," *IEEE Trans. Power Electron.*, vol. 28, no. 8, pp. 4104–4112, Aug. 2013.
[8] Q. Wang, G. Zhang, G. Wang, C. Li, and D. Xu, "Offline parameter self-learning method for general-purpose PMSM drives with estimation error compensation," *IEEE Trans. Power Electron.*, vol. 34, no. 11, pp. 11103–11115, Nov. 2019.
[9] S. A. Odhano et al., "Identification of three-phase IPM machine parameters using torque tests," *IEEE Trans. Ind. Appl.*, vol. 53, no. 3, pp. 1883–1891, May/Jun. 2017.
[10] K. Liu, Q. Zhang, J. Chen, Z. Q. Zhu, and J. Zhang, "Online multiparameter estimation of nonsalient-pole PM synchronous machines with temperature variation tracking," *IEEE Trans. Ind. Electron.*, vol. 58, no. 5, pp. 1776–1788, May 2011.
[11] G. Pellegrino, A. Vagati, P. Guglielmi, and B. Boazzo, "Performance comparison between surface-mounted and interior PM motor drives for electric vehicle application," *IEEE Trans. Ind. Electron.*, vol. 59, no. 2, pp. 803–811, Feb. 2012.
[12] Y. Shi, K. Sun, L. Huang, and Y. Li, "Online identification of permanent magnet flux based on extended Kalman Filter for IPMSM drive with position sensorless control," *IEEE Trans. Ind. Electron.*, vol. 59, no. 11, pp. 4169–4178, Nov. 2012.
[13] X. Li and R. Kennel, "General formulation of kalman-filter-based online parameter identification methods for VSI-fed PMSM," *IEEE Trans. Ind. Electron.*, vol. 68, no. 4, pp. 2856–2864, Apr. 2021.
[14] Y. Zhang, Z. Yin, X. Sun, and Y. Zhong, "On-line identification methods of parameters for permanent magnet synchronous motors based on cascade MRAS," in *Proc. 9th Int. Conf. Power Electron.-Energy Convers. Congr. Expo. Asia*, 2015, pp. 345–353.
[15] T. Boileau, N. Leboeuf, B. Nahid-Mobarakeh, and F. Meibody-Tabar, "Online identification of PMSM parameters: Parameter identifiability and estimator comparative study," *IEEE Trans. Ind. Appl.*, vol. 47, no. 4, pp. 1944–1957, Jul./Aug. 2011.
[16] M. X. Bui, M. F. Rahman, D. Guan, and D. Xiao, "A new and fast method for on-line estimation of d and q axes inductances of interior permanent magnet synchronous machines using measurements of current derivatives and inverter DC-Bus voltage," *IEEE Trans. Ind. Electron.*, vol. 66, no. 10, pp. 7488–7497, Oct. 2019.
[17] Z. Li, G. Feng, C. Lai, D. Banerjee, W. Li, and N. C. Kar, "Current injection-based multi-parameter estimation for dual three-phase IPMSM considering VSI nonlinearity," *IEEE Trans. Transp. Electrific.*, vol. 5, no. 2, pp. 405–415, Jun. 2019.
[18] S. Ichikawa, M. Tomita, S. Doki, and S. Okuma, "Sensorless control of permanent-magnet synchronous motors using online parameter identification based on system identification theory," *IEEE Trans. Ind. Electron.*, vol. 53, no. 2, pp. 363–372, Apr. 2006.
[19] D. Q. Dang, M. S. Rafaq, H. H. Choi, and J.-W. Jung, "Online parameter estimation technique for adaptive control applications of interior PM synchronous motor drives," *IEEE Trans. Ind. Electron.*, vol. 63, no. 3, pp. 1438–1449, Mar. 2016.
[20] S. Po-ngam and S. Sangwongwanich, "Stability and dynamic performance Improvement of adaptive full-order observers for sensorless PMSM drive," *IEEE Trans. Power Electron.*, vol. 27, no. 2, pp. 588–600, Feb. 2012.
[21] M. A. Hamida, J. De Leon, A. Glumineau, and R. Boisliveau, "An adaptive interconnected observer for sensorless control of PM synchronous motors with online parameter identification," *IEEE Trans. Ind. Electron.*, vol. 60, no. 2, pp. 739–748, Feb. 2013.
[22] X. G. Zhang and Z. X. Li, "Sliding-mode observer-based mechanical parameter estimation for permanent magnet synchronous motor," *IEEE Trans. Power Electron.*, vol. 31, no. 8, pp. 5732–5745, Aug. 2016.
[23] D. Liang, J. Li, R. Qu, and W. Kong, "Adaptive second-order sliding-mode observer for PMSM sensorless control considering VSI nonlinearity," *IEEE Trans. Power Electron.*, vol. 33, no. 10, pp. 8994–9004, Oct. 2018.
[24] X. Zhang, B. Hou, and Y. Mei, "Deadbeat predictive current control of permanent-magnet synchronous motors with stator current and disturbance observer," *IEEE Trans. Power Electron.*, vol. 32, no. 5, pp. 3818–3834, May 2017.
[25] M. Wlas, Z. Krzeminski, and H. A. Toliyat, "Neural-network-based parameter estimations of induction motors," *IEEE Trans. Ind. Electron.*, vol. 55, no. 4, pp. 1783–1794, Apr. 2008.
[26] W. Song, Y. Gang, Q. Zhi-Jian, S. Shuang-shuang, and C. Chao, "Identification of PMSM based on EKF and Elman neural network," in *Proc. IEEE Int. Conf. Autom. Logistics*, 2009, pp. 1459–1463.
[27] S. Zhao, Y. Peng, Y. Zhang, and H. Wang, "Parameter estimation of power electronic converters with physics-informed machine learning," *IEEE Trans. Power Electron.*, vol. 37, no. 10, pp. 11567–11578, Oct. 2022.
[28] F. Harashima, Y. Demizu, S. Kondo, and H. Hashimoto, "Application of neutral networks to power converter control," in *Proc. Conf. Rec. IEEE Ind. Appl. Soc. Annu. Meeting*, 1989, vol. 1, pp. 1086–1091.
[29] S. Mihai et al., "Digital twins: A survey on enabling technologies, challenges, trends and future prospects," *IEEE Commun. Surv. Tut.*, vol. 24, no. 4, pp. 2255–2291, Fourthquarter 2022.
[30] P. Jain, J. Poon, J. P. Singh, C. Spanos, S. R. Sanders, and S. K. Panda, "A digital twin approach for fault diagnosis in distributed photovoltaic systems," *IEEE Trans. Power Electron.*, vol. 35, no. 1, pp. 940–956, Jan. 2020.
[31] M. Milton, C. D. L. O, H. L. Ginn, and A. Benigni, "Controller-embeddable probabilistic real-time digital twins for power electronic converter diagnostics," *IEEE Trans. Power Electron.*, vol. 35, no. 9, pp. 9850–9864, Sep. 2020.
[32] Y. Peng, S. Zhao, and H. Wang, "A digital twin based estimation method for health indicators of DC–DC converters," *IEEE Trans. Power Electron.*, vol. 36, no. 2, pp. 2105–2118, Feb. 2021.
[33] Y. Liu, G. Chen, Y. Liu, L. Mo, and X. Qing, "Condition monitoring of power electronics converters based on digital twin," in *Proc. IEEE 3rd Int. Conf. Circuits Syst.*, 2021, pp. 190–195.
[34] Q. Wu, W. Wang, Q. Wang, L. Xiao, and B. Hu, "Digital twin approach for degradation parameters identification of a single-phase DC-AC inverter," in *Prpc. IEEE Appl. Power Electron. Conf. Expo.*, 2022, pp. 1725–1730.
[35] H. Shi, L. Xiao, Q. Wu, and W. Wang, "Digital twin approach for IGBT parameters identification of a three-phase DC-AC inverter," in *Proc. IEEE Transp. Electrific. Conf. Expo, Asia-Pacific*, 2022, pp. 1–4.
[36] X. Liu, C. Bentheimer, F. Hilpert, M. Hofmann, B. Eckardt, and M. Maerz, "Digital twin for a 10 MW electrical drive system for future electric aircraft applications," in *Proc. 11th Int. Electric Drives Prod. Conf.*, 2021, pp. 1–9.
[37] M. Ibrahim, V. Rjabtšikov, S. Jegorov, A. Rassõlkin, T. Vaimann, and A. Kallaste, "Conceptual modelling of an EV-permanent magnet synchronous motor digital twin," in *Proc. IEEE 20th Int. Power Electron. Motion Control Conf.*, 2022, pp. 156–160.
[38] Z. Chen, D. Liang, S. Jia, L. Yang, and S. Yang, "Incipient interturn short-circuit fault diagnosis of permanent magnet synchronous motors based on the data-driven digital twin model," *IEEE J. Emerg. Sel. Topics Power Electron.*, vol. 11, no. 3, pp. 3514–3524, Jun. 2023.
[39] Y. Yue, L. Cao, J. Hu, S. Cai, B. Hang, and H. Wu, "A novel hybrid location algorithm based on chaotic particle swarm optimization for mobile position estimation," *IEEE Access*, vol. 7, pp. 58541–58552, 2019.

Wensheng Song (Senior Member, IEEE) received the B.S. degree in electronic and information engineering and the Ph.D. degree in electrical engineering from Southwest Jiaotong University, Chengdu, China, in 2006 and 2011, respectively.

From 2009 to 2010, he was a Visiting Scholar with the Department of Electrical Engineering and Computer Science, University of California at Irvine, Irvine, CA, USA. From July 2015 to December 2015, he was a Visiting Scholar with the University of Alberta, Edmonton, AB, Canada. He is currently a Full Professor with the School of Electrical Engineering, Southwest Jiaotong University. His current research interests include power electronics, motor drives, health monitoring, and reliability of railway traction drive systems.

Yuchao Zou received the B.Eng. degree in electrical engineering from Eastchina Jiaotong University, Nanchang, China, in 2021. He is currently working toward the Masters's degree in electrical engineering with the Department of Electrical Engineering, Southwest Jiaotong University, Chengdu, China.

His current research interests include digital twin and PMSM.

Chenwei Ma (Member, IEEE) was born in China. He received the Ph.D. degree in electromechanical engineering from Ghent University, Ghent, Belgium, in 2021.

He has been with the Department of Electromechanical, Systems and Metal Engineering, Ghent University as a Postdoctoral Researcher since 2021. In 2022, he joined the Department of Electrical Engineering, Southwest Jiaotong University, Chengdu, China, where he is currently an Assistant Professor. His current research interests include motor drives, model predictive control, and data-driven techniques applied to power converters and electric drives.

Sihui Zhang (Student Member, IEEE) was born in Hebei Province, China, in 1998. She received the B.S. degree in electrical engineering, in 2020, from Southwest Jiaotong University, Chengdu, China, where she is currently working toward the Ph.D. degree in electrical engineering.

Her current research interests include state perception, monitoring, and reliability improvement of traction converters.